JOINT INSTITUTE FOR NUCLEAR RESEARCH

Veksler and Baldin Laboratory of High Energy Physics

FINAL REPORT ON THE SUMMER STUDENT PROGRAM

Study of elliptic and triangular flow in Au+Au collisions at $\sqrt{s_{NN}} = 11.5$ GeV and 14.5 GeV energies at STAR experiment

Supervisor: Alexey Aparin, JINR

Student: Alexey Povarov, Russia
National Research Nuclear Uiversity MEPhI

Participation Period: August 01 - September 14

Dubna, 2019

Abstract

Intensive investigation of the QCD phase diagram became of interest for many heavy ion experiments over the past two decades. One of the key features of matter produced in such collisions is a phase transition from usual nuclear matter to a new state of quasi-free quarks and gluons so called quark-gluon plasma. This work is dedicated to study of the elliptic and triangular flow at Au+Au collisions at the energies of BES-I programm at STAR experiment at Relativistic Heavy Ion Collider (RHIC). Flow is a measure of azimuthal anisotropy in heavy ion collisions and can be described by the respective coefficients of the azimuthal distribution Fourier decomposition. In this work results of collective flow study in Au+Au collisions at $\sqrt{s_{NN}} = 11.5$ GeV and 14.5 GeV energies are presented. Results obtained for elliptic flow υ_2 are in good agreement with the previous measurements made by STAR. In addition new measurements of triangular flow υ_3 are conducted fro this energies.

Contents

1. Introduction

Study of heavy ion collisions is actual and interesting objective. Theorists suggested a description for relativistic heavy ion collisions in terms of relativistic hydrodynamics around half a century ago [1]. Their ideas were confirmed in experiments on the collision of nuclei of heavy elements at the end of the last century. Relativistic Heavy Ion Collider (RHIC) was launched in the beginning of the 21-st century. It was built to create and study a new state of matter - Quark-Gluon Plasma (QGP). In QGP high density and temperature of nuclear substance are achieved, hence quarks and gluons can reach a state of deconfinement. This state was predicted in the quantum chromodynamics (QCD) [2]. A number of fundamental problems are associated with the study of the properties of quark-gluon plasma, such as phase transitions in nuclear matter and collective flow [3]. Phase transitions from the hadron phase to the state of the QGP can occur in highly heated or compressed nuclear matter.

The purpose of this work is to study collective flow (the second v_2 and third v_3 harmonics of the Fourier decomposition) in Au+Au collisions at $\sqrt{s_{NN}} = 11.5$ GeV and 14.5 GeV energies.

2. Theory Overview

2.1. QGP in heavy ion collisions

One of the major goals in high energy nuclear collisions is to determine the conditions behind the phase transition between hadronic matter (a state in which quarks and gluons are confined in composite particles, called baryons and mesons) and the QGP (a state of deconfined partonic matter). At high energies, Quantum Chromodynamics (QCD) predicts a phase transition, when hot and dense matter is melting, separating particles into a plasma where colored partons (quarks and gluons) became quasi-free and are no longer confined into colorless doublets (mesons) and triplets (barions).
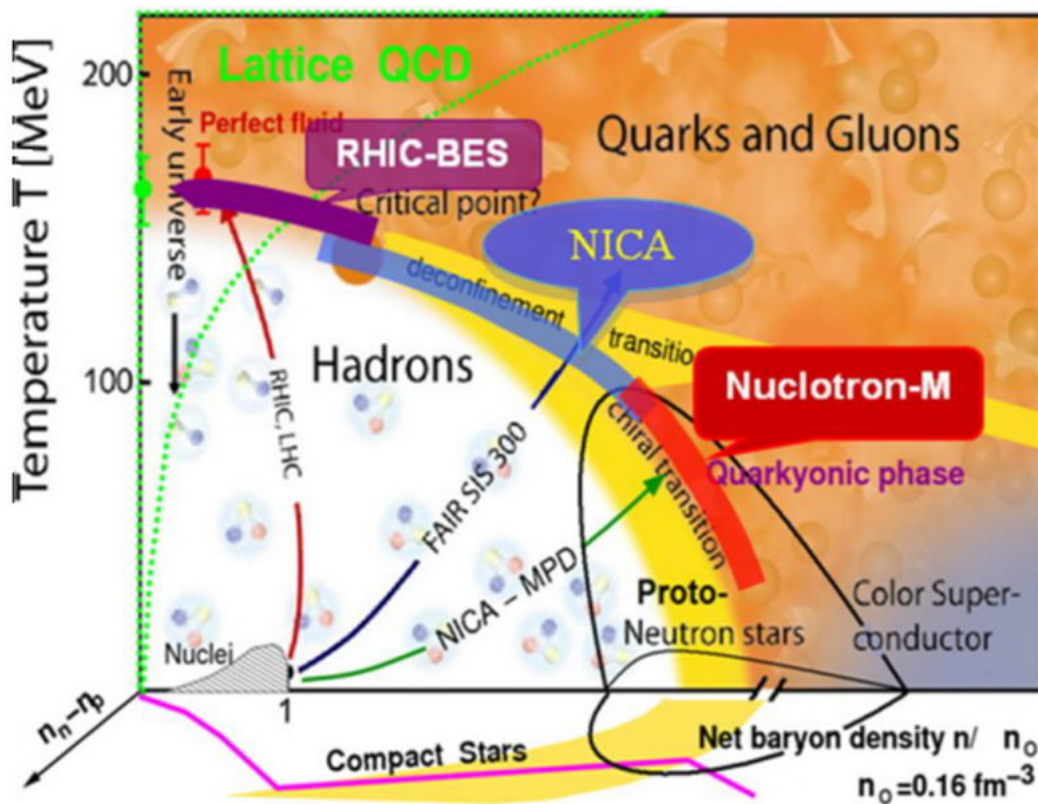

Figure 1. Phase diagram of nuclear matter

Phase diagram of nuclear matter is shown on Figure 1. Temperature T is plotted on the ordinate axis, and the density of baryonic matter on the abscissa axis. Quarks and gluons are in confinement state at low temperatures and densities of nuclear matter. This substance can be described as a hadron gas. With increasing temperature a nuclear matter transition is possible into state of deconfinement (fomation of QGP). QCD predict smooth cross-over phase transition at high temperatures and low baryon density, while a phirst order phase transition occures at high barion densities.

2.2. Azimuthal anisotropy

The analysis of azimuthal anisotropy arising in nucleus-nucleus collisions is an important area of modern high-energy physics. Azimuthal anisotropy provides information on the nature and properties of the substance formed in such collisions. Event plane anisotropy in particle momentum distribution is called collective flow. It has been studied since Bevalac experiments at Berkeley laboratory. Azimuthal anisotropy became even more interesting for scientists after experiments at AGS in Brookhaven, at SPS in CERN and at RHIC in Brookhaven. It made a push to creation of quark-gluon matter concept.

The analysis of azimuthal anisotropy is carried out using Fourier decomposition:

$$E\frac{d^3N}{d^3p} = \frac{1}{2\pi}\frac{d^2N}{p_t dp_t dy}(1 + \sum_{n=1}^{\infty} 2v_n \cos{(n(\phi - \Psi_r))}) \tag{1}$$

where E is a particle energy, p_T - transverse momentum of particle, y - rapidity, ϕ - particle azimuthal angle and Ψ_r - event plane angle.

The first harmonic coefficient corresponds to an overall shift of the distribution in the transverse plane; such flow is called directed flow v_1. It is the magnitude of the total vector sum of transverse momenta. In the case of negligible fluctuations the direction of flow due to symmetry should coincide with the reaction plane angle $\phi = \Psi_r$ (repulsive flow), or point in the opposite direction $\phi = \Psi_r + \pi$ (attractive flow).

The non-zero second harmonic describes the eccentricity of an ellipse-like distribution. If one approximates the distribution by an ellipse, then the second coefficient v_2 carries information on the magnitude of the eccentricity. Quantitatively it is the difference between the major and the minor axis.

Coefficient v_3 can be non-zero for asymmetric nuclear collisions and represent the asymmetry of the flow due to different sizes of colliding nuclei, if the distribution can be approximately described as triangle-type distribution [4].

3. STAR Experiment

The Solenoidal Tracker at RHIC (STAR) is one of two large detector systems constructed at the Relativistic Heavy Ion Collider at Brookhaven National Laboratory. STAR was constructed to investigate the behavior of strongly interacting matter at high energy density and to search for signatures of QGP formation [6]. The layout of the STAR experiment is shown in Figure 2.
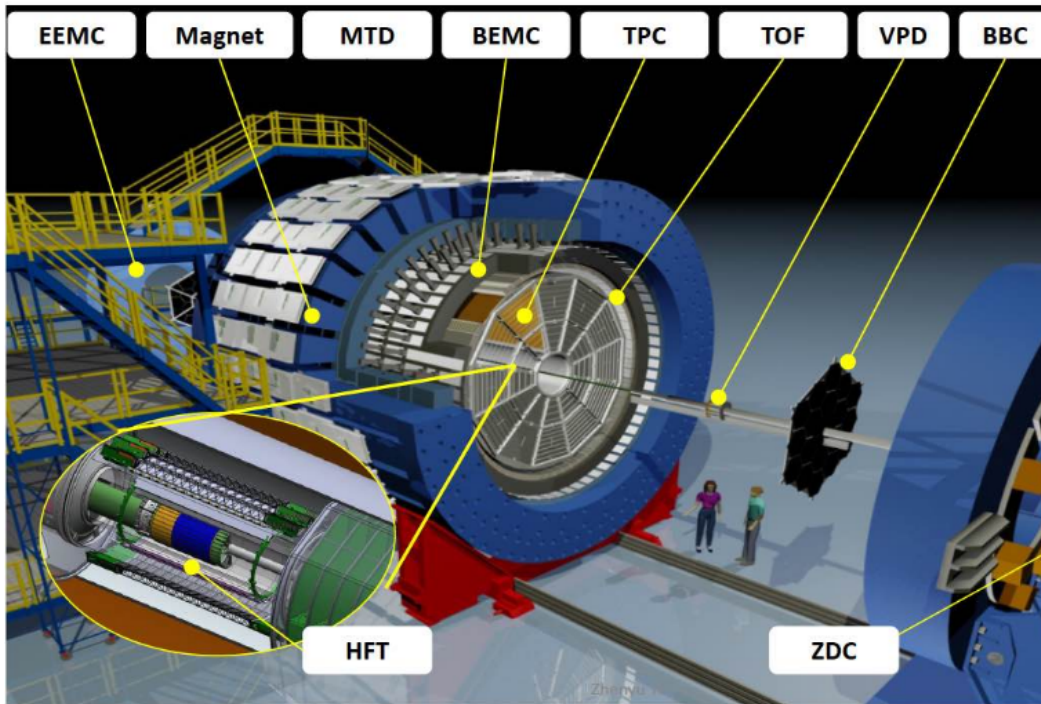

Figure 2. Perspective view of the STAR detector, with a cutaway for viewing inner detector systems.

STAR measures many observables simultaneously to study signatures of a possible QGP phase transition and to understand the space-time evolution of the collision process in ultra-relativistic heavy ion collisions. An experiment consists of several types of detectors. In this work Time Projection Chamber (TPC) and Time-of-Flight (TOF) system are used.

3.1. Time Projection Chamber

The STAR detector uses the TCP as it's primary tracking device. The TPC records the tracks of particles, measures their momenta, and identifies the particles by measuring their ionization energy loss (dE/dx). Its acceptance covers ± 1.8 units of pseudo-rapidity through the full azimuthal angle and over the full range of multiplicities. Particles are identified over a momentum range from 100 MeV/c to greater than 1 GeV/c; and momenta are measured over a range of 100 MeV/c to 30 GeV/c. The STAR TPC is shown schematically on Figure 3. It

sits in a large solenoidal magnet that operates at 0.5 T. The TPC is 4.2 m long and 4 m in diameter. It is an empty volume of gas in a well-defined, uniform, electric field of $\approx$ 135 V/cm.
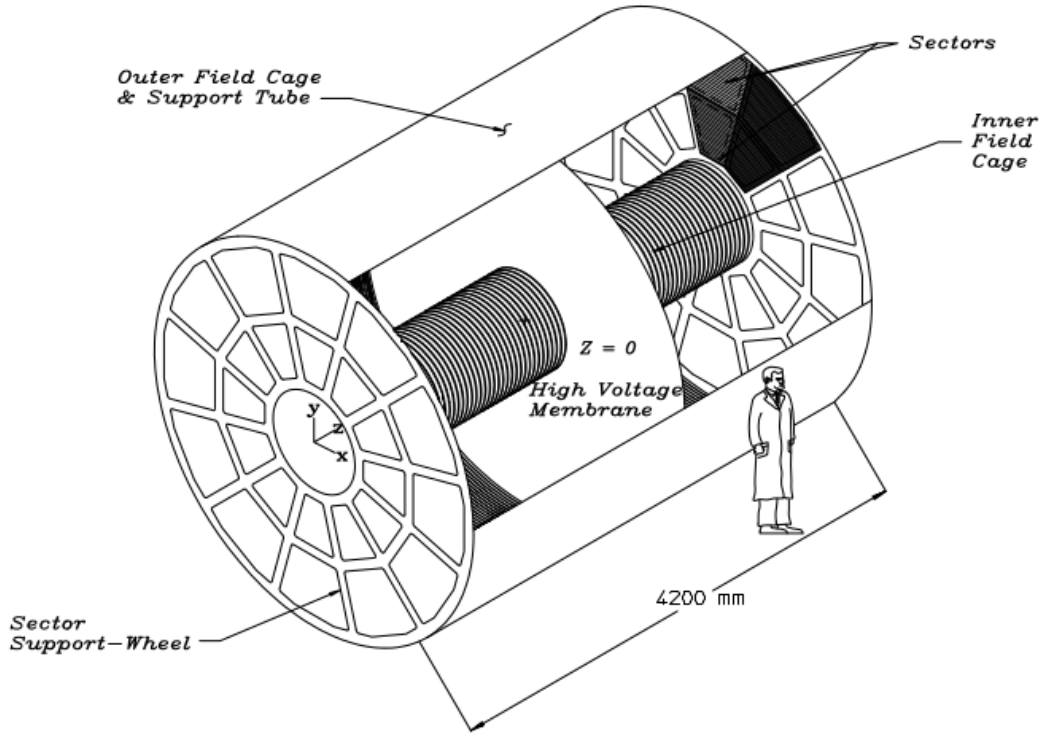

Figure 3. The scheme of STAR TPC surrounding the interaction region at RHIC.

The tracks of primary ionizing particles passing through the gas volume are reconstructed with high precision from the produced secondary electrons which drift to the readout end caps on the ends of the chamber. The uniform electric field which is required to drift the electrons is defined by a thin conductive Central Membrane (CM) at the center of the TPC, concentric field-cage cylinders and the readout end caps. Electric field uniformity is critical since track reconstruction precision is submillimeter and electron drift paths are up to 2.1m [7].

3.2. Time of Flight

A segmented time-of-flight system (TOF) is used to increase the possibility of particle identification in the STAR detector complex. It is based on multigap resistive plate chambers (MRPCs). TOF has cylindrical form and placed around TPC. The system has an intrinsic timing resolution of $\sim$ 85 ps. It covers the full azimuth and a pseudorapidity range of $-0.9 < \eta < 0.9$. Time of particle's flight is used for particle identification. The particle mass squared, m^2, can be calculated using the measured TOF velocity and the reconstructed momentum from the TPC [8].

8

4. Method of measurement collective flow

4.1. Estimation of the reaction plane

There are different methods to measure collective flow. In this work Event Plane (EP) method is used. The method uses the anisotropic flow itself to determine the event plane. It also means that the event plane can be determined independently for each harmonic of the anisotropic flow. The event flow vector Q_n and the event plane angle Ψ_n from the n–th harmonic of the distribution are defined by the equations

$$Q_n \cos\left(n\Psi_n\right) = X_n = \sum_i \omega_i \cos(n\phi_i) \tag{2}$$

$$Q_n \sin\left(n\Psi_n\right) = Y_n = \sum_i \omega_i \sin(n\phi_i) \tag{3}$$

$$\Psi_n = \frac{1}{n} \arctan \frac{\sum_i \omega_i \sin(n\phi_i)}{\sum_i \omega_i \cos(n\phi_i)} \tag{4}$$

The sums go over the i particles used in the event plane determination and the ω_i are respected weights [5].

4.2. Event plane angle corrections

Biases due to the finite acceptance of the detector which cause the particles to be azimuthally anisotropic in the laboratory system can be removed by making the distribution of event planes isotropic in the laboratory system. The simplest way to do this is to re-center (Eq. 5) the distributions (X_n, Y_n) (Eqs. 2,3) by subtracting the (X_n, Y_n) values averaged over all events [5],[9].

$$Q_{x(y)}^{Recent} = Q_{x(y)} - \langle Q_{x(y)} \rangle \tag{5}$$

The main disadvantage of this method is that it does not remove higher harmonics from the resulting distribution of Ψ_n. If such harmonics are present then the method requires additional alignment of the event plane distribution. For this we use flattening procedure (Eq. 6).

$$\Psi_n^{Flattening} = \Psi_n^{Recent} + \Delta\Psi_n^{Recent} \tag{6}$$

where

$$\Delta\Psi_n^{Recent} = \sum_i^{i_{max}} \frac{2}{i}(-\langle \sin\left(in\Psi_n\right)\rangle \cos\left(in\Psi_n\right) + \langle \cos\left(in\Psi_n\right)\rangle \sin\left(in\Psi_n\right)) \tag{7}$$

In equation 7 i_{max} is the number of coefficients, n is the harmonic number. This method fits the unweighted laboratory distribution of the event planes, summed over all events, to a Fourier expansion and devises an event-by-event shifting of the planes needed to make the final distribution isotropic [5].

4.3. Collective flow measurement

The coefficients in the Fourier expansion of the azimuthal distributions with respect to the real reaction plane are then evaluated by dividing on the event plane resolution. Collective flow value is calculated by equation 8 after calculating event plane angle and corrections.

$$v_n = \frac{cos(n(\phi - \Psi_n))}{\sqrt{\langle \cos(n(\Psi_n^a - \Psi_n^b)) \rangle}} \tag{8}$$

Denominator value is called event plane resolution $Res\{\Psi_n\}$. The mean cosine values are less than one and thus this correction always increases the flow coefficients [9].

4.4. Non-flow correlations influence

In this work we are using 2Sub-Event method to reduce the non-flow correlations influence. Idea is that TPC is divided into two independent segments TPC^{east} $(\eta < 0)$ and TPC^{west} $(\eta > 0)$. Part where the collision occurs is deleted. For this we take range of pseudorapidity that is called eta gap. In calculation of resolution and flow, tracks from this range does not used. Then equation 8 and $Res\{\Psi_n\}$ will be written as:

$$Res\{\Psi_n\} = \sqrt{\langle \cos(n(\Psi_{n,\eta-} - \Psi_{n,\eta+})) \rangle} \tag{9}$$

$$v_n = \frac{cos(n(\phi_\pm - \Psi_{n,\mp}))}{\sqrt{\langle \cos(n(\Psi_{n,\eta-} - \Psi_{n,\eta+})) \rangle}} \tag{10}$$

where $\Psi_{n,\eta-}$, $\Psi_{n,\eta+}$ - are event plane angles for TPC^{east} and TPC^{west} respectively, $\phi_\pm$ - is azimuthal angle of east or west track.

5. Measurements of elliptic and triangular flow

5.1. Event and track selection

In this work, we used the data of Au+Au collisions at energies of 11.5 and 14.5 GeV per nucleon obtained in the STAR (RHIC). A set of cuts was applied to experimental data. A cut on the event vertex along the beam direction of ±50 cm and a cut on the event vertex radial displacement from the mean of 2 cm were made for 11.5 GeV. For 14.5 Gev the event vertex placement along the beam direction of ±70 cm and a cut on the event vertex radial displacement from the mean of 1 cm and Y-shift of 0.89 cm were made. The beam has shifted due to installation of a new detector. The events selection cuts and number of events after that are shown in the table 1.

Table 1. Event cuts and number of minimum bias events

DATA	no. events	Vertex$_z$	Vertex$_r$
Au+Au 11.5 GeV	10.2M	$|V_z| < 50$ cm	$|V_r| < 2$ cm
Au+Au 14.5 GeV	24.5M	$|V_z| < 70$ cm	$|V_r| < 1$ cm

The tracks used in the analysis are primary tracks. In order to ensure accurate track momentum reconstruction, short tracks were eliminated from the analysis by requiring all tracks to have a minimum number of 15 fit points in the TPC. The effect of track-splitting by the tracking algorithm is minimized by further requiring that the number of fit points is more than a half (0.52) of the total possible hit points number for a track in TPC. To avoid admixture of tracks from secondary vertices, a requirement is placed on the distance of closest approach (DCA) between each track and the event vertex. All tracks were also required to be within a pseudorapidity range of $|\eta| < 1.0$. The summary of all track selection criteria is listed in Table 2.

Table 2. Track selection cuts

Track parameter	value
Distance of closest approach	DCA < 3.0 cm
No. of fit points	nHitsFit > 15
nHitsFit/nHitsPoss	Ratio $\geqslant 0.52$
Pseudorapidity	$|\eta| < 1.0$

In this work event and track cuts coincide with cuts that were used in previous measurements of the elliptic flow [8],[10].
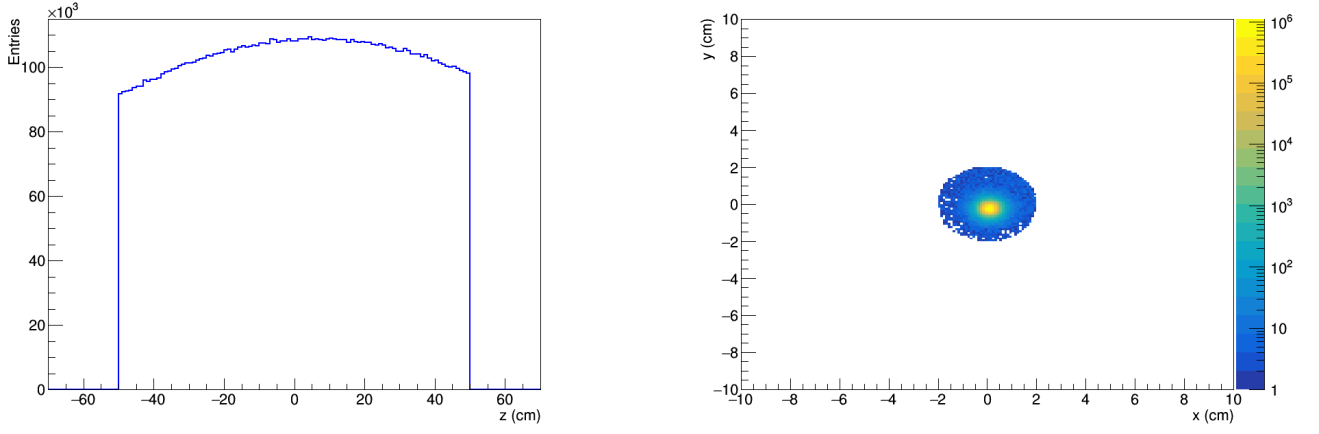
Figure 4. Distribution of Z-component of event vertex (left panel) and $\sqrt{V_x^2 + V_y^2}$ (right panel) after cuts for Au+Au collisions at $\sqrt{s_{NN}} = 11.5$ GeV
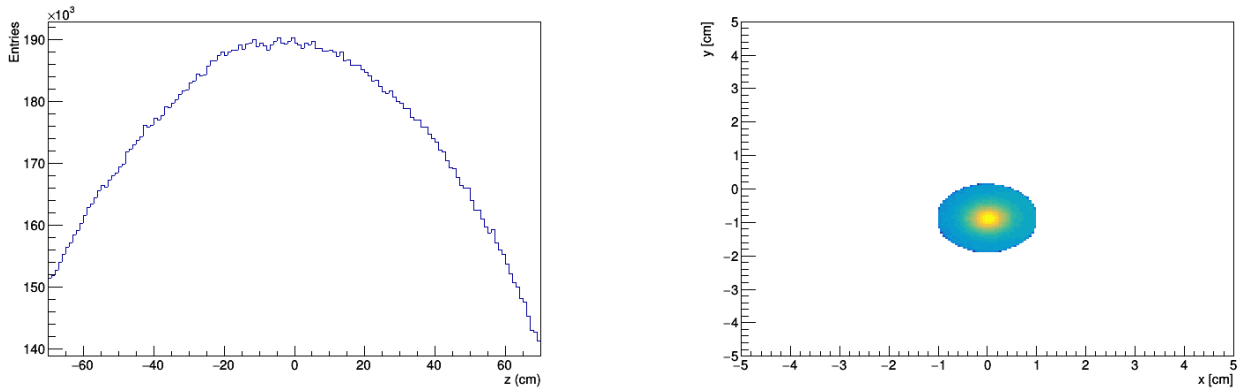

Figure 5. Distribution of Z-component of event vertex (left panel) and $\sqrt{V_x^2 + V_y^2}$ (right panel) after cuts for Au+Au collisions at $\sqrt{s_{NN}} = 14.5$ GeV

Distributions of average values of multiplicity, TOF tray multiplicity, Z-component of event vertex, transverse momentum, energy loss, azimuthal angle, number of hits by RunID were obtained, since data taking was going on for some time. Then standard deviation of average values and it's errors was calculated for given distributions. Run was not taken into analysis if calculated values were beyond three standard deviations. Below are some examples of distributions for each energy.
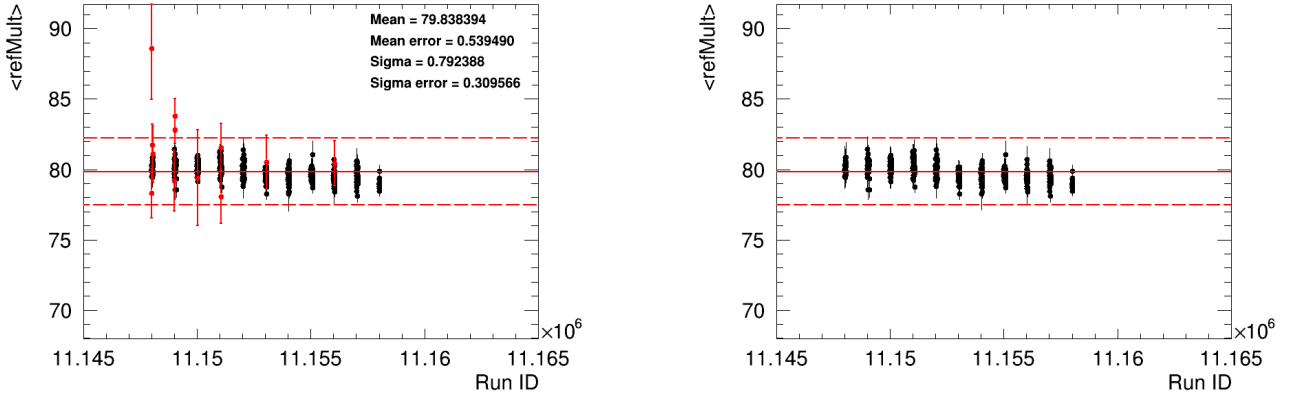
Figure 6. Distribution of multiplicity for Au+Au collisions at $\sqrt{s_{NN}} = 11.5$ GeV
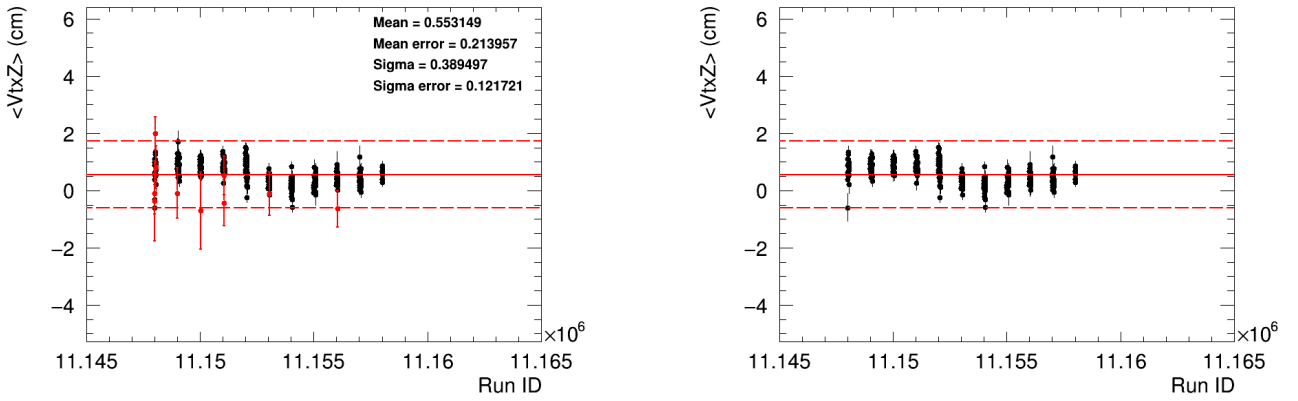
Figure 7. Distribution of Z-component of event vertex for Au+Au collisions at $\sqrt{s_{NN}} = 11.5$ GeV
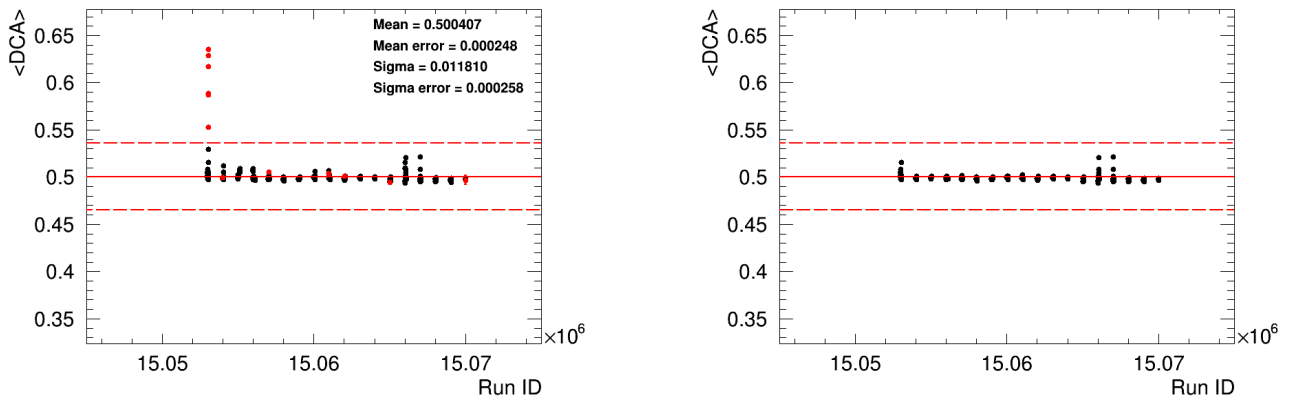
Figure 8. Distribution of distance closest approach for Au+Au collisions at $\sqrt{s_{NN}} = 14.5$ GeV

13

5.2. Calculation of the event plane resolution

The resolutions for second and third harmonics were obtained by Equation 9 with η-gap 0.1. The dependence of resolution on centrality is shown for each energy in Figure 9.
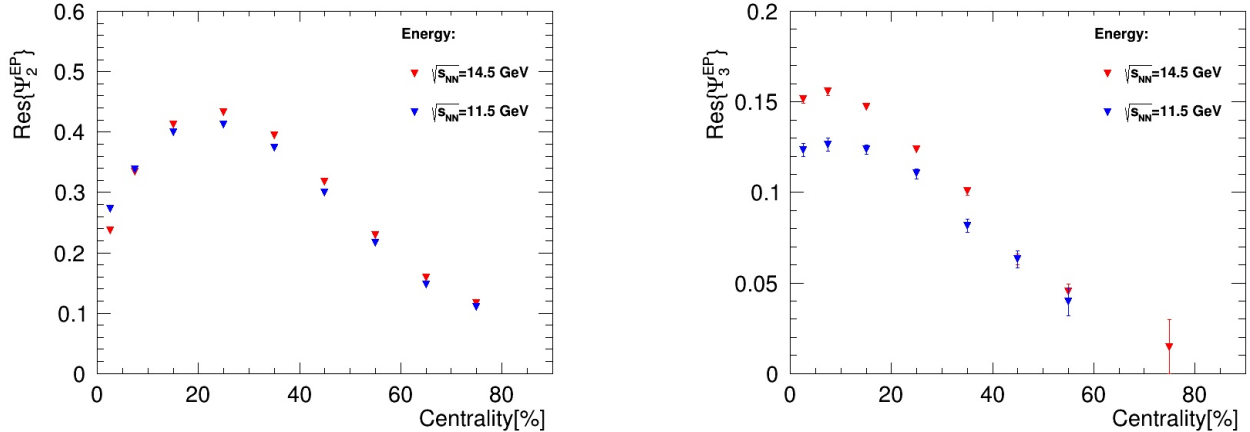
Figure 9. Event plane resolution for second and third harmonics of the flow

The event plane resolution is proportional to the flow coefficient times the square root of the particle multiplicity. It decreases with decreasing beam energy due to the lower particle multiplicities. $\text{Res}\{\Psi_2\}$ has a maximum for each beam energy at about 20-30% centrality. For more peripheral events, the relatively low multiplicity is responsible for the decreasing resolution, whereas for more central events the small flow signal is. The event plane resolution for third harmonic decreases with decreasing beam energy as well. It doesn't have distinct maximum and decreases for more peripheral events.

5.3. Elliptic flow

The values of the elliptical and triangular flows were calculated by Eq. 10 using resolution of event plane obtained in the previous paragraph. Figures 10 show dependence of the elliptic flow on transverse momentum for several centralities of Au+Au collisions at $\sqrt{s_{NN}} = 11.5$ GeV for charged hadrons. Figure 11 show the same for Au+Au collisions at $\sqrt{s_{NN}} = 14.5$ GeV. A comparison of the obtained values was made with previous elliptic flow measurements [8], [10]. All values are within the margin of error. We can conclude that this method works correctly. A more precise picture of convergence of values can be obtained from v_2 (p_T) ratios. The elliptic flow v_2 grows monotonically with the increase of transverse momentum p_T. The v_2 increases with p_T up to 1.5 GeV/c and reaches maximum value $\tilde{0}.23$ for peripheral collisions within the measured p_T range. Elliptic flow of identified handrons, namely pions, kaons and proton, was

also measured. Figure 12 shows a compared flow of particles and antiparticles for 0%-40% centrality Au+Au collisions at $\sqrt{s_{NN}} = 11.5, 14.5$ GeV. The bottom row of each panel shows the difference between a particle and corresponding antiparticle v_2 (p_T). The v_2 increases with p_T up to 1.5 GeV/c. In this graphs flow of π^- and K^- is higher than flow of π^+ and K^+, when p_T is more than 2.0 GeV/c. But the opposite was observed for p and $\bar{p}$. Figures 13 and 14 show elliptic flow v_2 for particles and antiparticles as a function of transverse momentum p_T for 0%-40% and 30%-60% centrality in Au+Au collisions at $\sqrt{s_{NN}} = 11.5, 14.5$ GeV.
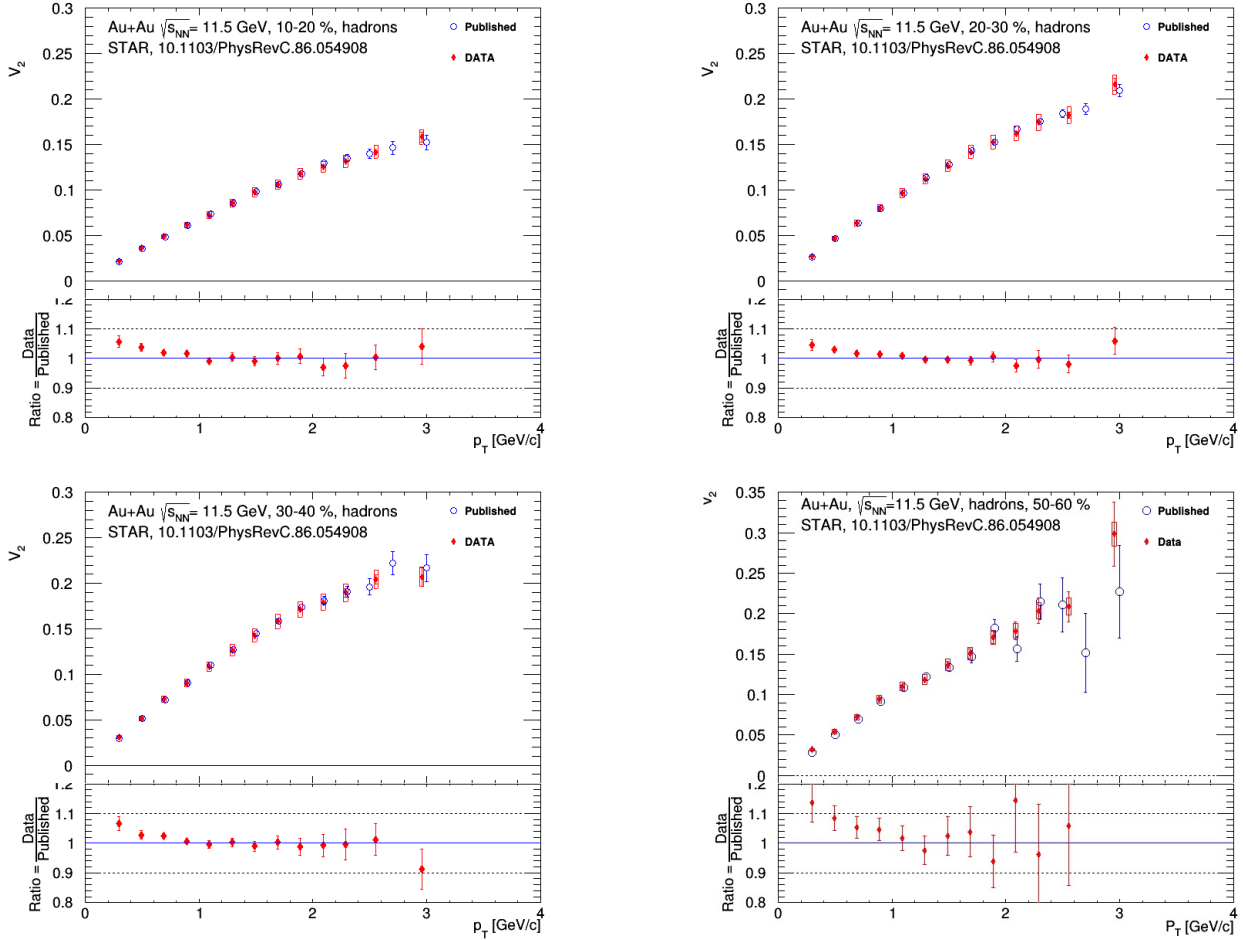
Figure 10. The elliptic flow, v_2, as a function of the transverse momentum, p_T, from different centrality of Au+Au collisions at $\sqrt{s_{NN}} = 11.5$ GeV for charged hadrons

Graphs below show that elliptic flow has a clear dependence on collision centrality and type of particles. Dependence on collision centrality appears due to $v2$ is sensitive to geometric form of the collision initial state.
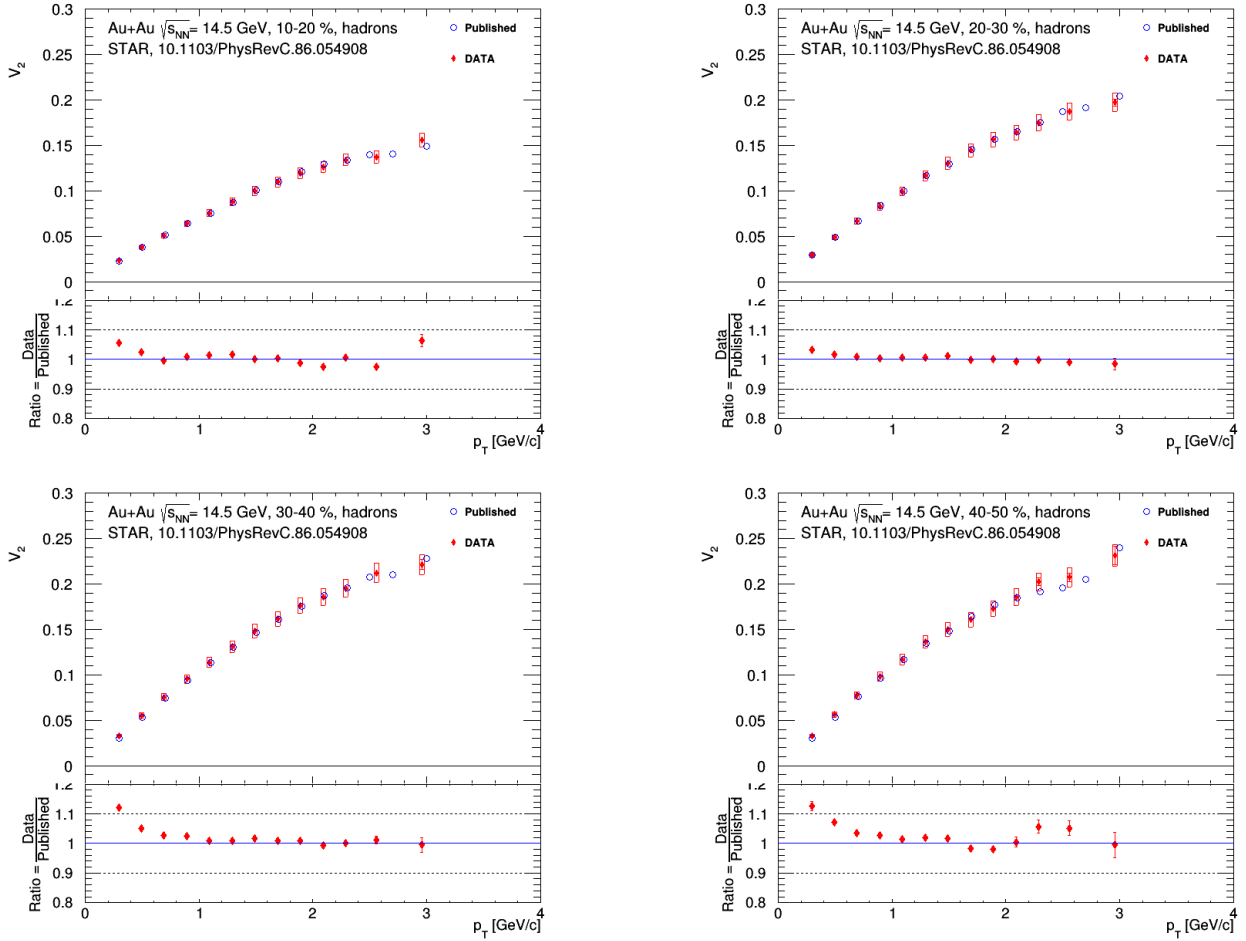
Figure 11. The elliptic flow, v_2, as a function of the transverse momentum, p_T, from different centrality of Au+Au collisions at $\sqrt{s_{NN}} = 14.5$ GeV for charged hadrons
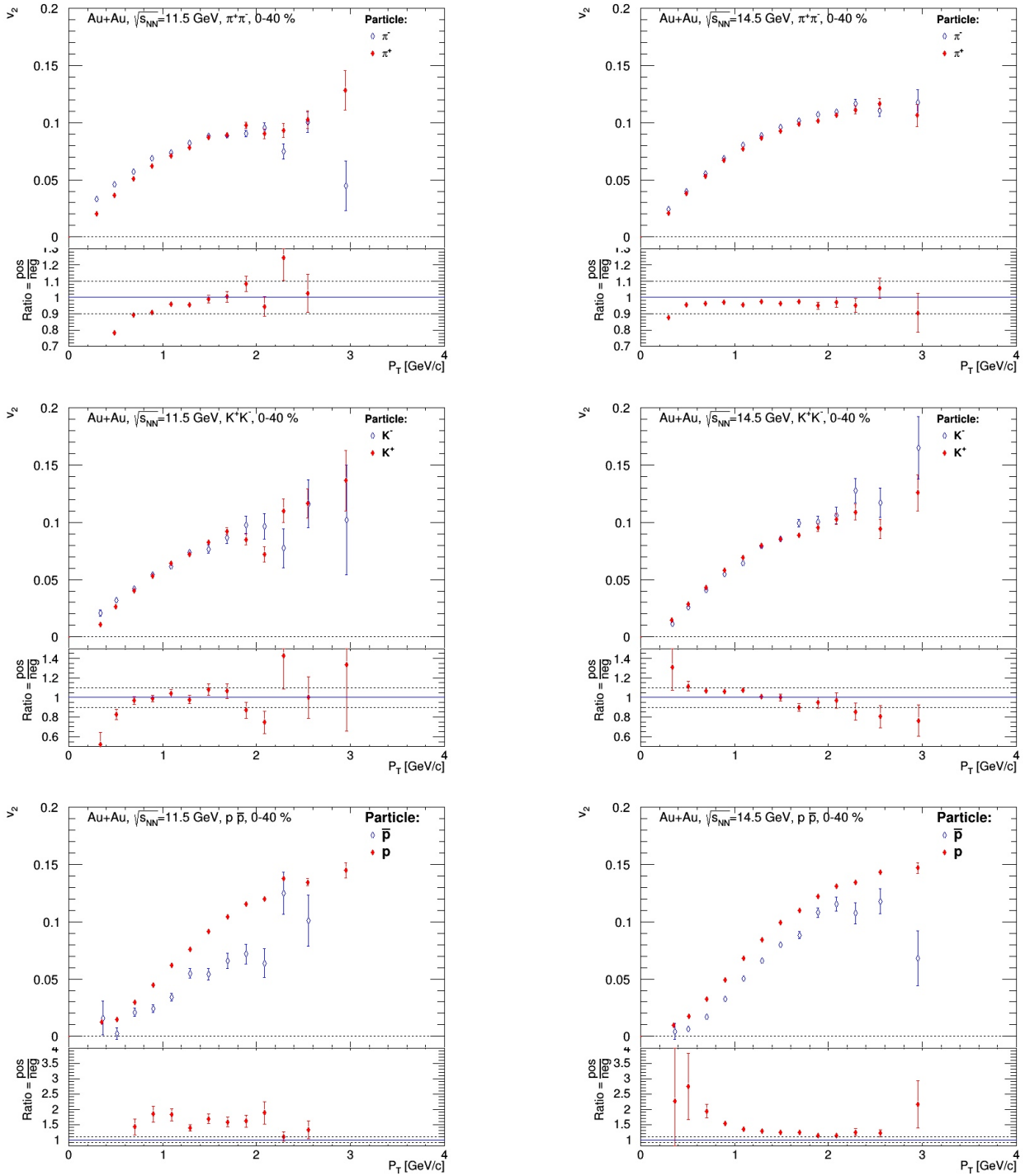
Figure 12. Elliptic flow, v_2, as a function of the transverse momentum, p_T, from different centrality of Au+Au collisions for various particle species and energies: on the left - for Au+Au collisions at $\sqrt{s_{NN}} = 11.5$ GeV, on the right - $\sqrt{s_{NN}} = 14.5$ GeV
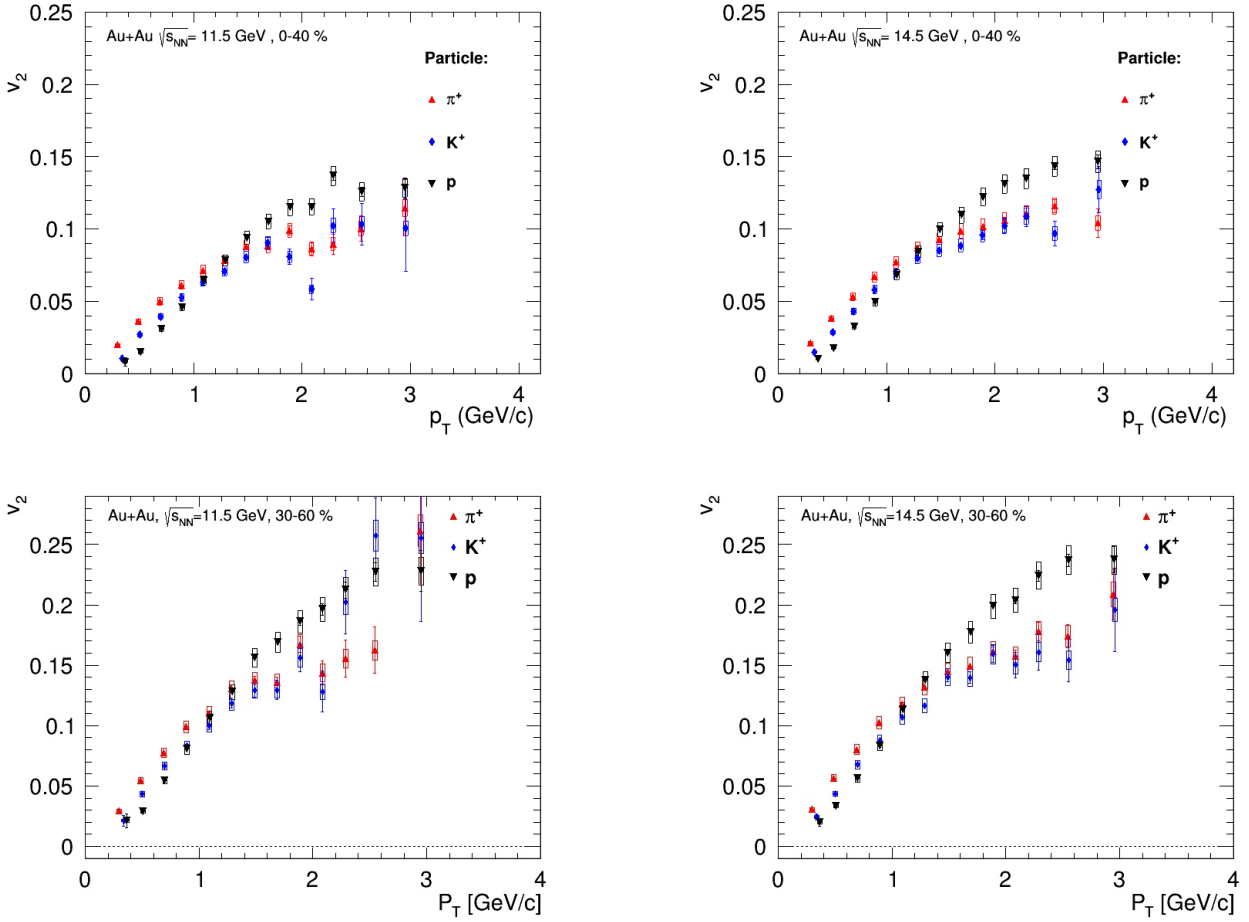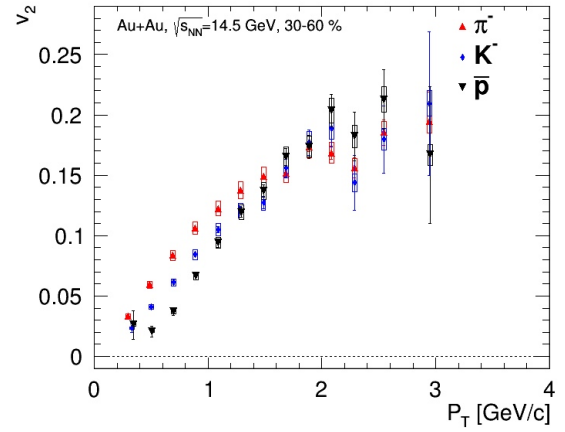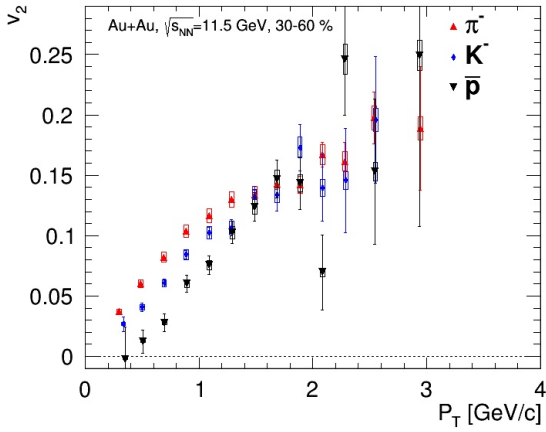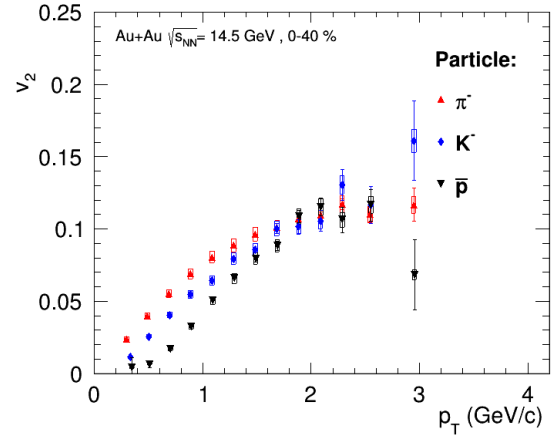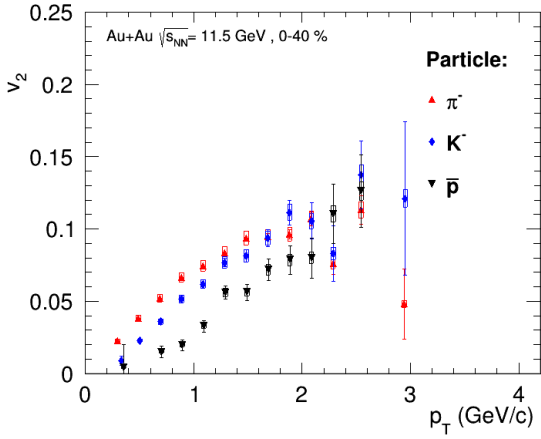
Figure 13. Elliptic flow, v_2, of positively charged particles as a function of the transverse momentum, p_T, for 0-40%, 30-60% centrality of Au+Au collisions for various particle species and energies: on the left - for Au+Au collisions at $\sqrt{s_{NN}} = 11.5$ GeV, on the right - $\sqrt{s_{NN}} = 14.5$ GeV

Figure 14. Elliptic flow, v_2, of negatively charged particles as a function of the transverse momentum, p_T, 0-40%, 30-60% centrality of Au+Au collisions for various particle species and energies: on the left - for Au+Au collisions at $\sqrt{s_{NN}} = 11.5$ GeV, on the right - $\sqrt{s_{NN}} = 14.5$ GeV

5.4. Triangular flow

The measured values of triangular flow v_3 are new for these energies. Figures 15 and 16 show dependencies of triangular flow v_3 on transverse momentum, p_T for 0%-10%, 10%-40%, 40%-80%, 0%-60% centrality of Au+Au collisions at $\sqrt{s_{NN}} = 11.5, 14.5$ GeV. Triangular flow v_3 of identified handrons, namely pions, kaons and proton, was also measured. Figure 17 shows compared flow of particles and antiparticles for 0%-40% centrality of Au+Au collisions at $\sqrt{s_{NN}} = 11.5, 14.5$ GeV. Figures 18 and 19 show v_3 for particles and antiparticles as a function of transverse momentum p_T for 0%-40% centrality of Au+Au collisions at $\sqrt{s_{NN}} = 11.5, 14.5$ GeV.
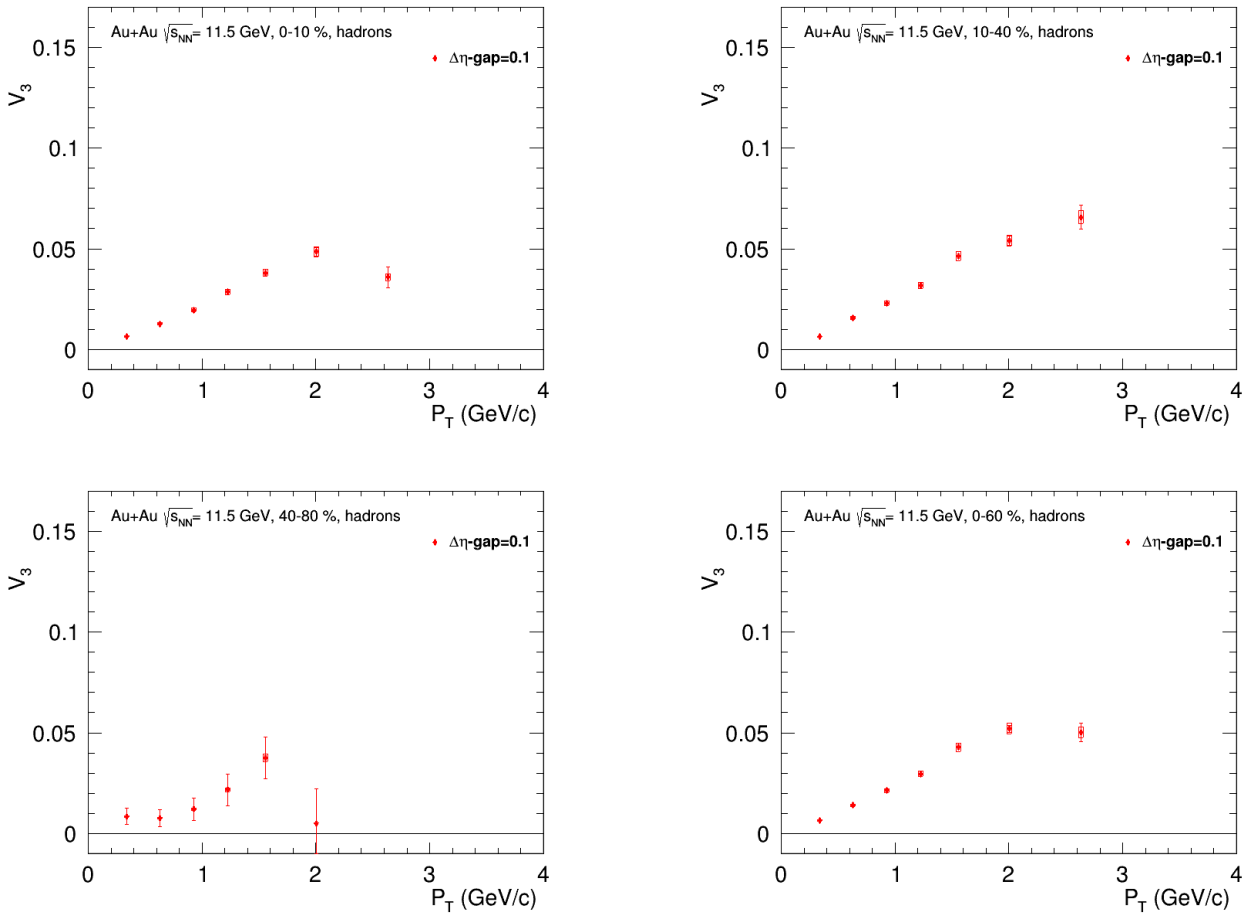
Figure 15. Triangular flow, v_3, of charged hadrons as a function of the transverse momentum, p_T, for different centrality of Au+Au collisions at $\sqrt{s_{NN}} = 11.5$ GeV

From these graphs one can see that triangular flow v_3 weakly depends on the centrality of the collision and type of particles. This confirms the suggestion that v_3 is sensitive to nucleon fluctuations and does not depend on the collision geometry as elliptic flow v_2.
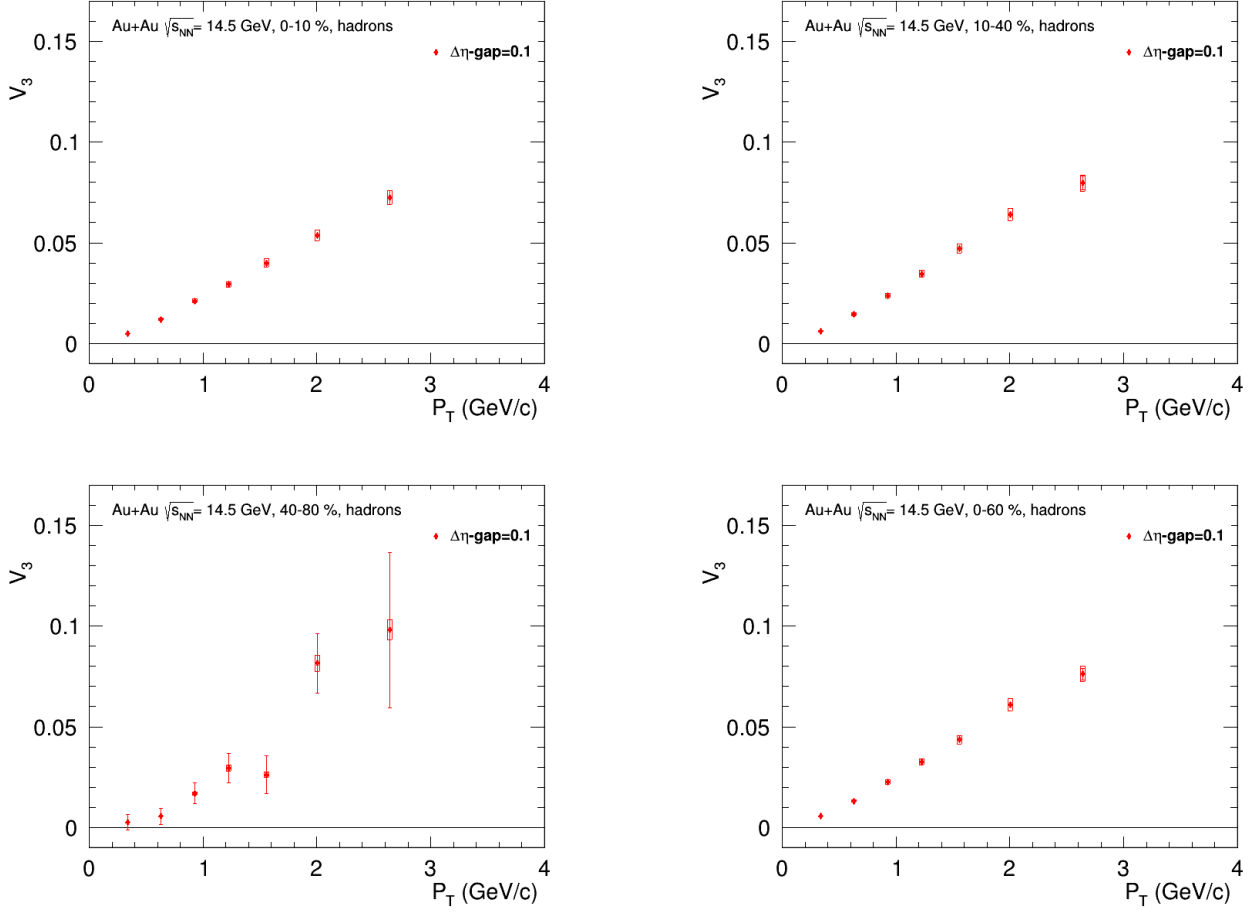
Figure 16. Triangular flow, v_3, of charged hadrons as a function of the transverse momentum, p_T, for different centrality of Au+Au collisions at $\sqrt{s_{NN}} = 14.5$ GeV
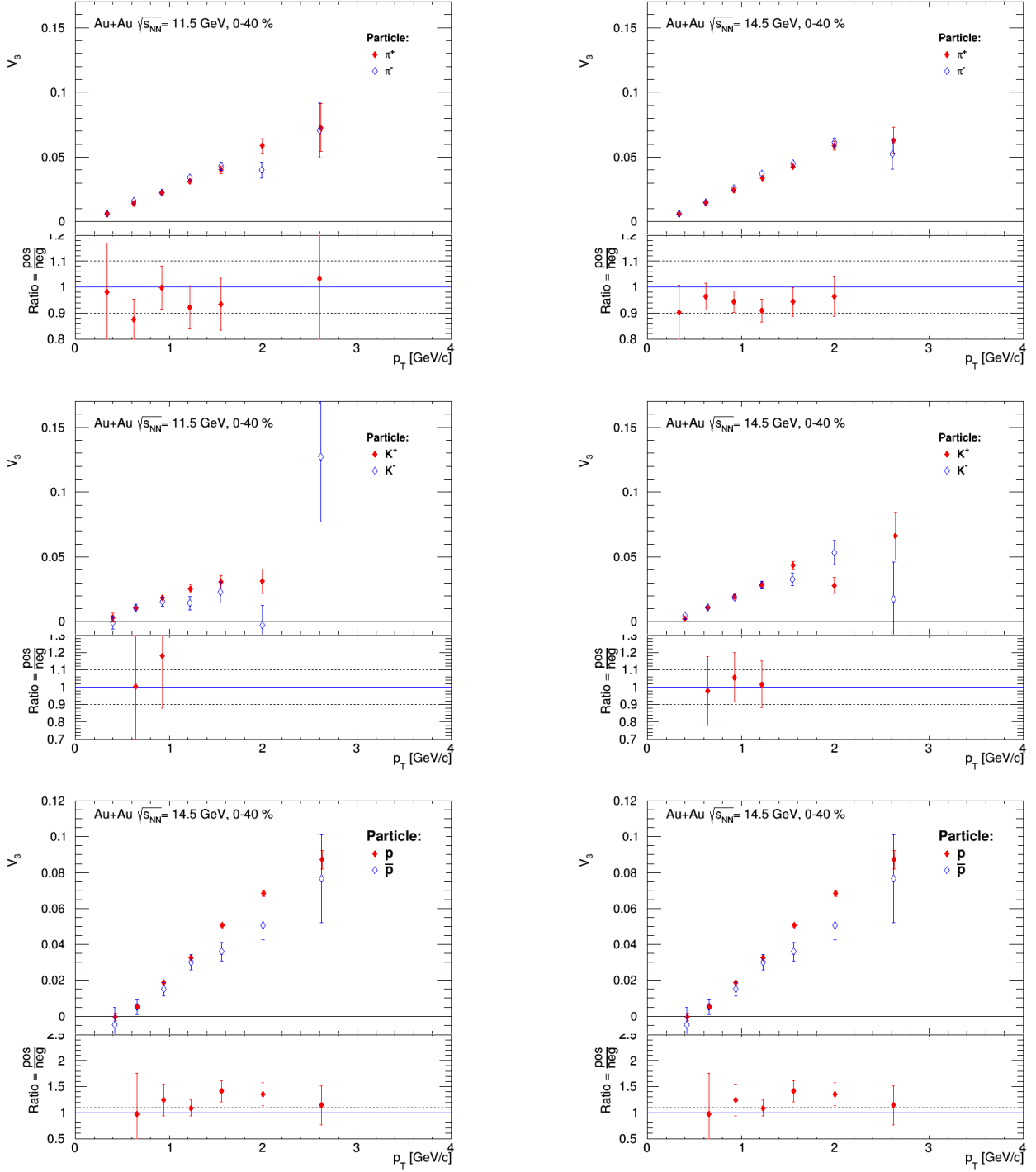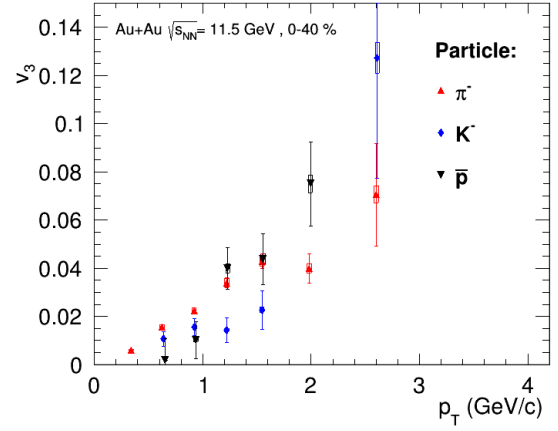
Figure 17. The triangular flow, v_3, as a function of the transverse momentum, p_T, for different centrality of Au+Au collisions for various particle species and energies: on the left - for Au+Au collisions at $\sqrt{s_{NN}} = 11.5$ GeV, on the right - $\sqrt{s_{NN}} = 14.5$ GeV
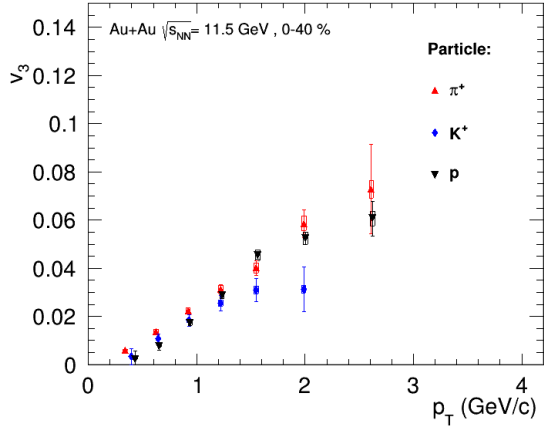
Figure 18. Triangular flow, v_3, of particles and antiparticles as a function of the transverse momentum, p_T, for 0-40% centrality of Au+Au collisions at $\sqrt{s_{NN}} = 11.5$ GeV
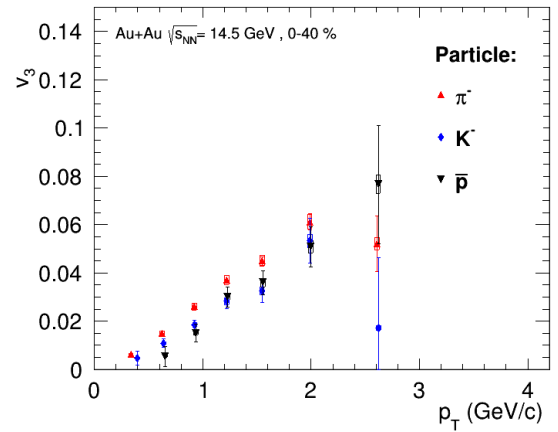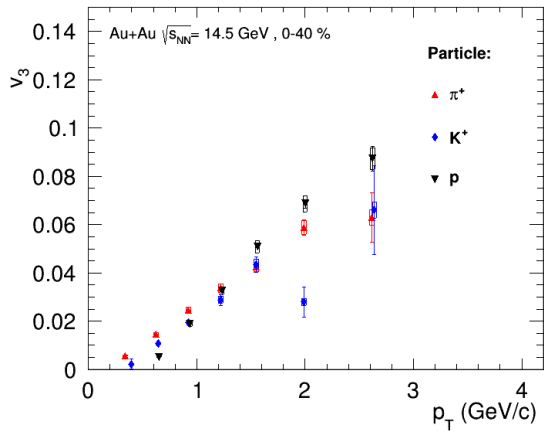

Figure 19. Triangular flow, v_3, of particles and antiparticles as a function of the transverse momentum, p_T, for 0-40% centrality of Au+Au collisions at $\sqrt{s_{NN}} = 14.5$ GeV

5.5. Comparison of the elliptic and triangular flow

Below mentioned figures show comparison of elliptic flow v_2 and triangular flow v_3 as a function of transverse p_T momentum for several centralities of Au+Au collisions at $\sqrt{s_{NN}} = 11.5, 14.5$ GeV. In these graphs, the dependence of v_2 on centrality in comparison with v_3 is clearly visible.
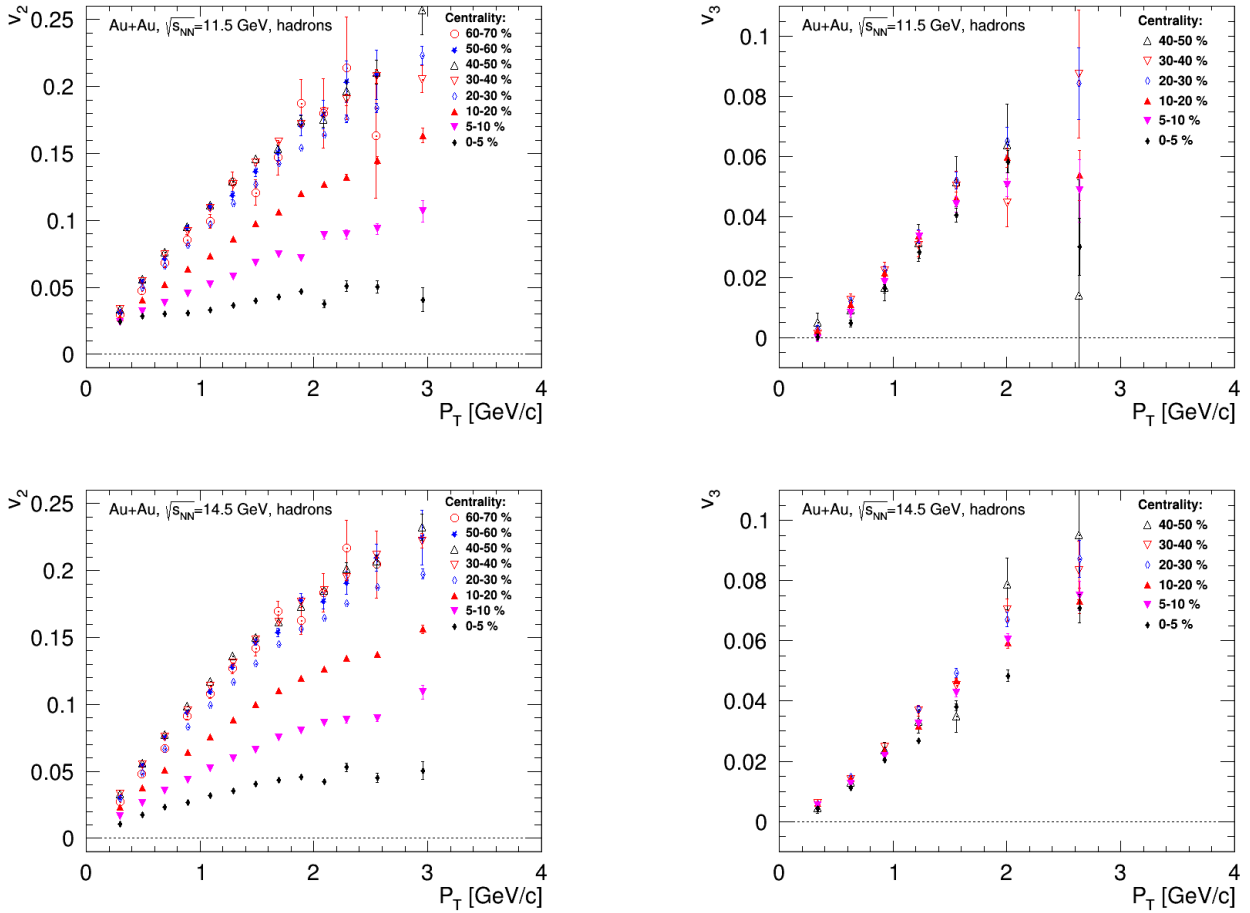

Figure 20. Comparison of the elliptic v_2 and triangular v_3 flow as function of transverse momentum p_T for several centralities of Au+Au collisions at $\sqrt{s_{NN}} = 11.5, 14.5$ GeV

6. Conclusion

In this work, we studied the elliptic v_2 and triangular v_3 flow of charged and indentified hadrons. An analysis was made for the Au+Au collisions at 11.5 and 14.5 GeV per nucleon, obtained on the STAR detector at RHIC. The elliptic flow values for charged and identified hadrons were obtained, dependence of v_2 on the transverse momentum in the range from 0.2 to 3.0 GeV/c for various centralities was calculated, and a comparison was made with STAR data to verify the recovery method for measuring the collective flow. Values coincide within the margin of error. The results of the triangular v_3 flow for charged and identify hadrons, new for this energies, were obtained and the dependence of v_3 as a function of transverse momentum for several centralities was calculated. The graphs show the dependence of the elliptic flow on centrality. This indicates that it depends on the geometric shape of the initial collision state. The dependence on the type of particles is also visible. The triangular flow does not have these dependencies because it depends o nucleons density fluctuations.

7. Acknowledgements

References

[1] D.J. Gross, F. Wilczek, Phys. Rev. Lett. 30, 1343, 1973.

[2] Korotkikh V.L. Quark-gluon plasma effects in collisions of relativistic ions. Moscow: published house KDU, 2018. p. 148

[3] Dremin I.M., Leonidov A.V., Quark-gluon medium, Uspekhi Fizicheskikh Nauk, No. 11, 2010.

[4] S. Voloshin, Y. Zhang, "Flow Study in Relativistic Nuclear Collisions by Fourier Expansion of Azimuthal Particle Distributions", Z. Phys. C70, p. 665-672, 1996.

[5] A.M. Poskanzer, S.A. Voloshin, "Methods for analyzing anisotropic flow in relativistic nuclear collisions", Phys. Rev. C58, 1671, 1998.

[6] K.H. Ackermann, et al., "STAR detector overview", Nuclear Instruments and Methods in Physics Research Section A, 499 (2003), 624-632.

[7] K.H. Ackermann, et al., "The STAR Time Projection Chamber: A Unique Tool for Studying High Multiplicity Events at RHIC", Nuclear Instruments and Methods in Physics Research Section A, 499 (2003), 659-678.

[8] L. Adamczyk, et al., "Elliptic flow of identified hadrons in Au+Au collisions at $\sqrt{s_{NN}}$ = 7.7-62.4 GeV", Phys. Rev. C88, 014902, 2013.

[9] Ilya Selyuzhenkov, Sergei Voloshin, "Effects of non-uniform acceptance in anisotropic flow measurement", Phys. Rev. C77, 034904, 2007.

[10] L. Adamczyk, et al., "Centrality dependence of identified particle elliptic flow in relativistic heavy ion collisions at $\sqrt{s_{NN}}$ = 7.7-62.4 GeV", Phys. Rev. C93, 014907, 2016.